Збірник наукових праць. Галузеве машинобудування, будівництво
Academic journal. Industrial Machine Building, Civil Engineering
http://journals.nupp.edu.ua/znp
https://doi.org/10.26906/znp.2025.64.4144

UDC 624.012

**Petro Reznik ***
O.M. Beketov National University of Urban Economy in Kharkiv
https://orcid.org/0000-0003-3937-6833

**Dmytro Petrenko**
O.M. Beketov National University of Urban Economy in Kharkiv
https://orcid.org/0000-0002-8168-7224

**Anton Volodymyrov**
O.M. Beketov National University of Urban Economy in Kharkiv
https://orcid.org/0009-0001-8416-535X

**Dzhamaldii Alataiev**
O.M. Beketov National University of Urban Economy in Kharkiv
https://orcid.org/0000-0003-1570-8469

# Flexural Behaviour of 3DCP Beams with Expanded Metal Sheet Reinforcement: Experimental Investigation and Numerical Verification

Abstract. An experimental and numerical study of the flexural behavior of 3D-printed concrete (3DCP) beams reinforced with expanded metal sheet are presented in this paper. Four-point bending tests on beams of 3DCP were carried out in accordance with DSTU B V.2.7-214:2009, recording load–deflection curves and strains. The 3DCP showed an equivalent axial tensile strength 30–45 % lower than that of class C16/20 concrete. Correctly oriented sheet reinforcement increased failure load and flexural toughness by about 30–40 %, while a 3D FE model in LIRA-FEM reproduced ultimate loads within 5–10 % but underestimated stiffness.

Keywords: 3D-printed concrete (3DCP); flexural tensile strength; expanded metal sheet; finite-element modelling; permanent formwork.

*Corresponding author E-mail: Petro.Reznik@kname.edu.ua



Received: 16.05.2025 Accepted: 06.06.2025 Published: 26.06.2025

**Introduction.**

Extrusion-based 3D printing of concrete has, over the last decade, evolved from an experimental technique into one of the key directions in digital construction. The studies [1–3] outline the basic stages of the extrusion process, formulate a research roadmap for 3D concrete printing (3DCP), and show that the combination of robotic material deposition, digital design and tailored rheological properties opens up possibilities for creating geometrically complex and structurally efficient members. Review papers [4,5] systematise the requirements for printable mixes, their rheology, mechanical and durability properties, and emphasise that predicting the load-bearing capacity and crack resistance of 3D-printed elements requires a dedicated approach compared with traditional cast-in-place concrete.

One of the fundamental features of 3D-printed cementitious composites is the anisotropy of mechanical properties caused by the layered build-up and the orientation of fibres or defects in the structure. The works [6,7] propose quantitative approaches to assessing the anisotropy of strength and deformability of 3D-printed mortars and concretes. Experimental studies [8–11] show that fibre orientation and content, extrusion-process parameters and modification with nanoadmixtures directly affect the ratio between the strength along the layers and that in the direction perpendicular to the layers. At the same time, earlier research on 3D printing of cement-based compositions [12,13] demonstrates that even at the level of powder-based or high-strength printable mixtures, specific mechanical responses are formed that are characteristic of the additive process and differ from those of conventional concretes.

A separate body of research is devoted to early-age and interlayer strength of 3D-printed concrete. The study [14] shows that early-age mechanical behaviour

governs the maximum buildable wall height without failure of the underlying layers, whereas [15] provides a detailed analysis of the influence of process parameters on the adhesion between layers in the hardened state. Investigations [16,17] indicate that the surface condition, the time interval between layers, moisture content and additional technological treatments can either substantially increase or markedly reduce interlayer bond strength. The works [18,19] complement this picture by linking porosity, internal stiffness contrast, fibre orientation and shrinkage processes with reduced crack resistance and local stress concentrations in 3D-printed elements.

For assessing the stress–strain state and refining experimental data, numerical models that account for material anisotropy and failure mechanisms are increasingly employed. In [20], the anisotropic flexural behaviour of fibre-reinforced 3D-printed concrete was investigated, and the role of printing direction in crack formation was demonstrated. Numerical analysis in [21] shows that anisotropy can be incorporated into finite element models used to describe the behaviour of specimens in compression and bending, which is an important step towards transferring laboratory test results into practical design of real structural members.

Building on the progress in 3DCP, approaches to the development of thin-walled members and 3D-printed formwork are being actively proposed. The review [22] systematises state-of-the-art solutions that utilise 3D-printed moulds for concrete elements, highlighting the advantages of complex geometries, reduced material consumption and the integration of service voids. Studies [23,24] demonstrate the potential of digitally fabricated ribbed slabs produced with 3D-printed formwork, which makes it possible to significantly reduce slab self-weight and material usage while maintaining load-bearing capacity. Such solutions are highly sensitive to the tensile and flexural behaviour of concrete, especially in regions of pronounced bending and local stress concentrations.

On the basis of these findings, it can be concluded that, for the further development of frame systems with thin-walled elements and permanent formwork produced by 3D printing, it is crucial to reliably evaluate the tensile response of 3D-printed concrete, taking into account its anisotropic structure and interlayer effects. This need underpins the relevance of combined experimental and numerical studies aimed at determining the tensile strength of 3D-printed concrete and verifying the effectiveness of reinforcing thin-walled elements with expanded metal sheet that can be integrated into permanent 3D-printed formwork for frame structures.

**Problem statement.**

The aim of this study is to experimentally evaluate the tensile strength in bending of beam specimens made of 3D-printed concrete, to simultaneously assess the effectiveness of their reinforcement with expanded metal sheet (EMS), and to further verify the results by constructing a finite-element (FE) model of the member.

To achieve this aim, the following main tasks were formulated:

- prepare four series of specimens made of 3D-printed and cast concrete in the form of 100×100×400 mm prisms: series U – 3D-printed concrete without reinforcement; series M and M90 – 3D-printed concrete reinforced with EMS; series N – conventional concrete of class C20/25.
- carry out experimental tests on flexural tension of beams made of 3D-printed concrete and C20/25 concrete in accordance with DSTU B V.2.7-214:2009 [25], recording the “load–deflection” diagrams and strains in the compression zone.
- based on the obtained results, determine the ultimate strength of the specimens, the failure load and failure pattern, and analyse the influence of EMS orientation on load-bearing capacity, deformability and failure mode.
- perform numerical modelling of the beams in Lira-FEM 2024, taking into account the properties of 3D-printed concrete and the three-dimensional behaviour of the members, and verify the model by comparing it with the experimental results.

**Main material and results.**

For the production of slabs (Fig. 1a) from which the beam specimens were cut, a dry mix Ceresit CN 278 3D Printing was used. The mechanical properties of this material under 3D printing were previously investigated in [27]. For cubes and prisms cut from large-scale printed elements, the following average compressive strengths were obtained: about 12.3 MPa in the X-direction, 12.4 MPa in the Y-direction and 17.3 MPa in the Z-direction, perpendicular to the layers [27]. Thus the actual strength level of the 3D-printed concrete corresponds to class C16/20 with pronounced anisotropy between the horizontal and vertical loading directions. For comparison with the “3D-printed” concrete, two control beams were cast from conventional normal-weight concrete of class C20/25.

As reinforcement, an extruded expanded metal sheet of type Sv 3.2×13.4×0.8 with a thickness of 0.6 mm made of cold-rolled steel 08kp was used. The sheet has rhombic openings with dimensions of approximately 3.2×13.4 mm, which provide perforation and mechanical interlock with the concrete.

To incorporate this sheet into the finite-element model, it was replaced by an equivalent solid plate of thickness $t_{eq}$. The calculation was performed assuming conservation of the volume of steel per unit area. For the geometry of the sheet reduced to an initial solid plate of thickness $b_0 = 0.5$ mm, the theoretical mass is $m_{0,5} = 1113$ kg/m². With a steel density of $\rho = 7850$ kg/m³ the equivalent thickness is

$$t_{eq},0.5 = m_{0.5} / \rho \approx 0.142 \text{ mm} \quad (1)$$

The fraction of the area occupied by steel is

$$f = t_{eq},0.5 / b_0 \approx 0.28 \quad (2)$$

For the actual thickness of the initial sheet b = 0,6 mm the equivalent solid thickness is

$$t_{eq} = f \cdot b \approx 0.17 \text{ mm} \quad (3)$$

In the subsequent analysis, both for calculations and interpretation of the experiments, the expanded metal sheet is treated as a thin solid steel plate of thickness $t_{eq} \approx 0.17$ mm, located in the tensile zone of the beam.

Reinforcement with the expanded metal sheet was carried out at the stage of printing slabs with overall dimensions of 500×500×100 mm. The sheet was placed in the lower part of the slab, at a distance of about 20 mm from its bottom surface, over the entire plan area.

The sheet was laid in two orientations: with the long diagonal of the mesh aligned with the printing direction (series M), and perpendicular to the printing direction (series M90). Comparison of these two orientations makes it possible to assess the sensitivity of the system to the reinforcement direction and the degree to which the potential of the expanded metal sheet is utilised.

After hardening, the slabs with and without reinforcement were cut into beams with a nominal cross-section of 100×100 mm and a length of 400 mm, as shown in Fig. 1b. Before testing, the actual length, width and height of each specimen were measured in three sections, as well as its mass. These data were used to determine the average geometric dimensions and the average concrete density for each beam.

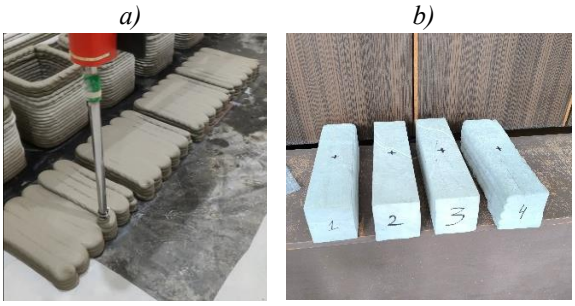


**Figure 1 – Process of 3D printing concrete slabs (a) and cutting prisms of size 100×100×400 mm from them (b)**

Flexural tests on the beams were carried out on a servo-driven electromechanical testing machine UTM STM-50 with a maximum load capacity of 50 kN. Load control and recording of the "load–deflection" diagrams were performed via a personal computer using dedicated software.

Flexural tensile tests on the beam specimens were performed in accordance with DSTU B V.2.7-214:2009 [25]. The prisms were installed in a special loading frame following the scheme shown in Fig. 2: the specimen rested on two hinged supports with a span between the support balls of l = 3a, where is the side of the square cross-section.

For a cross-section of approximately 100×100 mm, the span was 300 mm. The load was applied at two points located at a distance of one third of the span from each support, by means of a distributing spreader beam. In this way, a four-point bending scheme with a constant bending moment in the central third of the span and zero transverse force in that zone was realised.

Longitudinal strains in the beams were measured using foil resistance strain gauges connected to a multichannel data-acquisition system VNIИ-8.

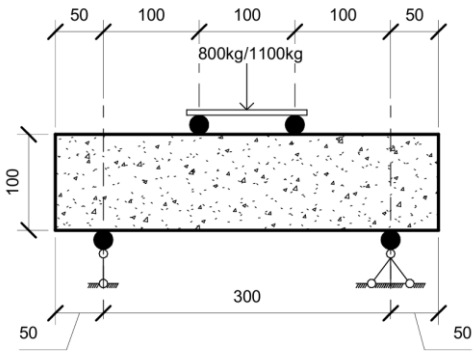


**Figure 2 – Test set-up for prisms in flexural tension**

Longitudinal strains in the beams were measured using foil resistance strain gauges connected to a multichannel data-acquisition system VNIИ-8. The strain gauges were bonded at mid-span on the top and bottom surfaces of the beam along its axis. In addition, mid-span deflections were recorded using a dial gauge with a resolution of 0.001 mm. Figure 3a shows a specimen installed in the testing machine, and Fig. 3b – a specimen at the moment of failure.

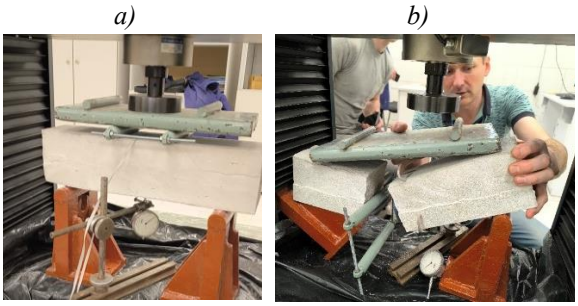


**Figure 3 – Four-point bending test of 3D-printed concrete beams: (a) instrumented specimen in the testing machine; (b) specimen at the moment of failure**

The results of determining the ultimate loads for the specimens of the different series are presented in Fig. 4.

The maximum failure loads for the four specimens of series U were within a range corresponding to applied forces of approximately 7.0–9.0 kN. This indicates that the ultimate loads are significantly lower than for the control specimens made of conventional concrete of higher strength class. For the specimens of series M, the failure loads were in the range of about 11.0–12.6 kN. The mean value was about 11.5 kN, which greatly exceeds the average failure load of series U (about 8.0 kN). For the specimens of series M90, the failure loads were concentrated in the interval of about 8.0–9.0 kN, with an average value of approximately 8.4 kN. This is only slightly higher than the value for the unreinforced series U (about 8.0 kN) and is considerably lower than for series M.

The flexural tensile strength $f_{c,tf}$ for each specimen was calculated in accordance with [25]. The design

tensile strength of concrete, taking into account the conversion from flexural strength to the conventional axial tensile strength with a factor $k_1$=0.55, was in the range from 1.02 to 1.25 MPa (Fig. 5).

The obtained values of the equivalent axial tensile strength are lower than those expected for concrete of class C16/20, which corresponds to the compressive strength level of the 3D-printed mixture used. According to [28], the characteristic tensile strength for C16/20 is $f_{ctm}$=1.9 MPa. Thus, the effective tensile strength of the investigated 3D-printed concrete is reduced by approximately 30–45 % compared with conventional cast concrete of the same class.

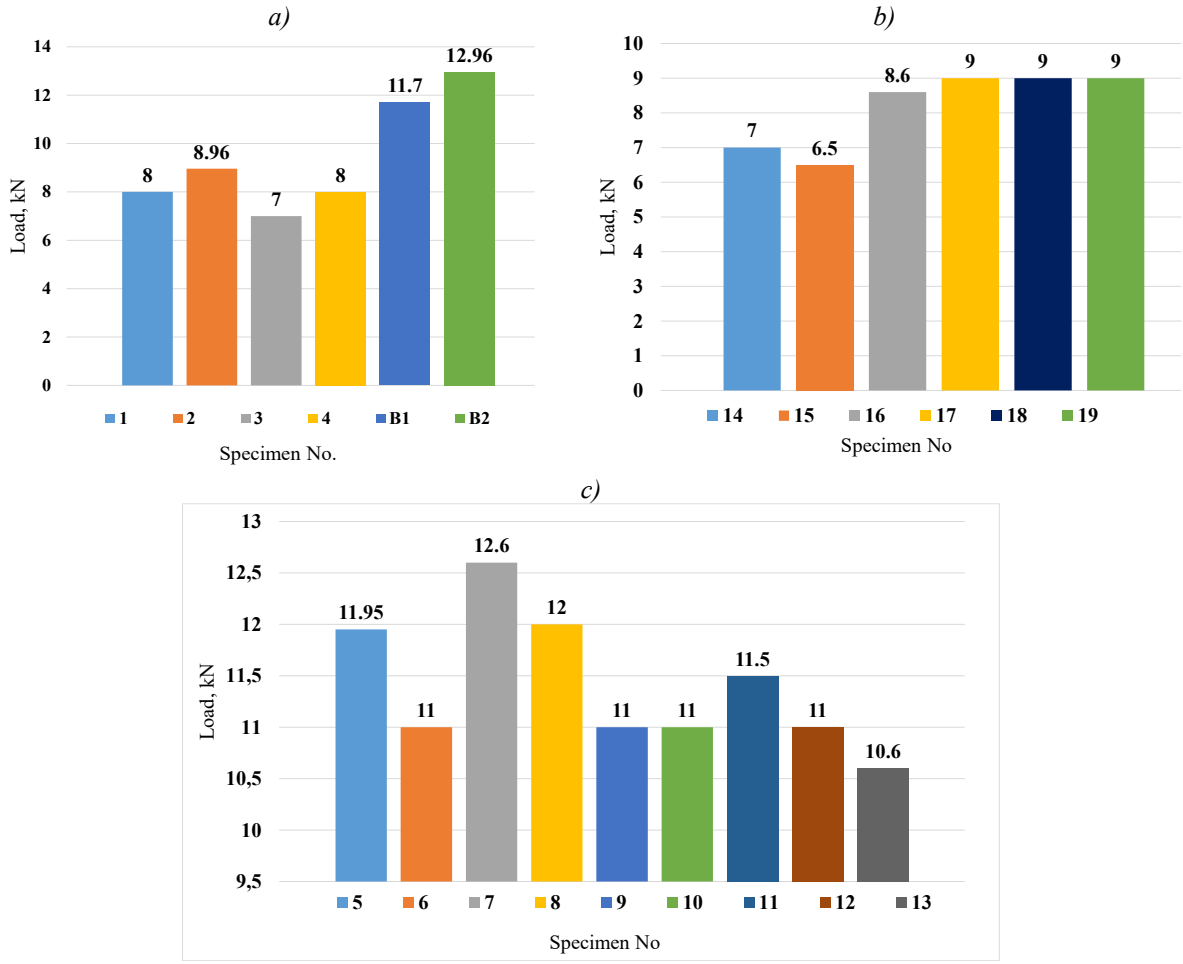


**Figure 4 – Maximum failure loads for beams of each series: (a) U – without reinforcement (specimens B1 and B2 are beams made of conventional concrete); (b) M90 – reinforced with EMS perpendicular to the extrusion direction; (c) M – reinforced with EMS along the extrusion direction**

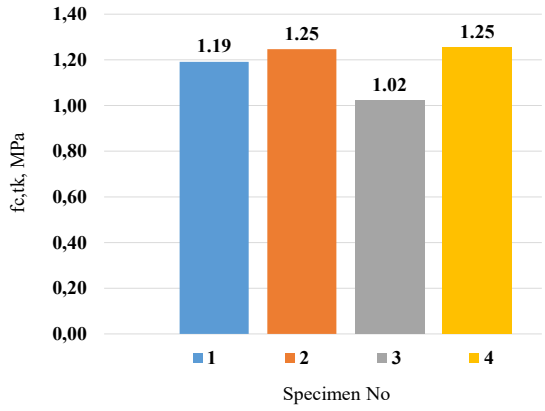


**Figure 5 – Flexural tensile strength $f_{c,tf}$ for individual specimens of series U**

Analysis of the strain-gauge measurements on the unreinforced specimens showed that, in the pre-cracking stage, the strains in the compression and tension zones are almost linear and of opposite sign, which corresponds to a symmetric curvature distribution with respect to the neutral axis. The formation of the first visible crack in the tension zone was recorded at strains, $\varepsilon_t \approx 0.10–0.15$ ‰, i.e. at a level close to the design limiting tensile strain $\varepsilon_{ctu} \approx 0.13$ ‰ for class C16/20. After cracking, the strain-gauge readings in the tension zone become more scattered and less reliable due to local crack opening and possible partial debonding of the gauges from the concrete surface.

The load–deflection diagrams F-w, plotted from dial-gauge readings at mid-span, are shown in Fig. 6a for series U. All specimens of this series exhibit an almost linear branch up to the formation of the first crack; afterwards, the stiffness decreases noticeably and then remains approximately constant up to failure

as the deflection increases. Visually, it is evident that the 3D-printed concrete has a lower flexural stiffness and a smaller ultimate deflection, which corresponds to a more brittle failure mode.

According to the test results, the failure loads of series M lay in the range of approximately 11.0–12.6 kN. The mean value of the maximum load is 11.5 kN, which is about 40–45 % higher than the mean ultimate load of the unreinforced series U. The deformation and failure behaviour of the reinforced specimens differed significantly from that of the unreinforced ones. In the diagram for series M (Fig. 6b), the central part of the curve corresponding to the development of inclined flexural cracks is accompanied by a substantial increase in deflection. The central zone of stress redistribution between concrete and sheet, bounded by the opening of the main crack and the involvement of adjacent regions in tension, confirms this picture.

For the reinforced specimens of series M, the compressive strains in the top zone (red curve) reach values of about 0.30–0.60 ‰, i.e. approximately two to three times higher than those recorded for the unreinforced beams at failure. Strains in the tension zone, measured by strain gauges, increase up to about 0.13 ‰ by the time the first through-crack forms.

In summary, it can be stated that, despite the very small equivalent thickness and relative reinforcement ratio of about 0.2 %, the expanded metal sheet with a favourable orientation significantly increases the load-bearing capacity and deformability of 3D-printed beams in bending. The increase in load-bearing capacity reaches approximately 40–45 %, and the presence of reinforcement, due to reduced crack susceptibility, enables further mobilisation of the energy capacity of 3DCP flexural members.

According to the test results for series M90 (Fig. 6c), the failure loads of these specimens are in the range of about 8.0–9.0 kN, with an average value of roughly 8.4 kN. This only slightly exceeds the mean ultimate load of series U and is considerably lower than that of series M. The load–deflection curves of series M90 are similar in shape to those of the unreinforced beams. Only at the attainment of the maximum load does the curve drop sharply, which corresponds to a local peak effect similar to that observed in series M. This indicates the absence of a pronounced additional contribution of the sheet reinforcement to the deformation response. The tests also record only a minor increase in ultimate deflections; therefore, the deformability of elements with the sheet oriented perpendicular to the extrusion direction is almost the same as that of the unreinforced specimens.

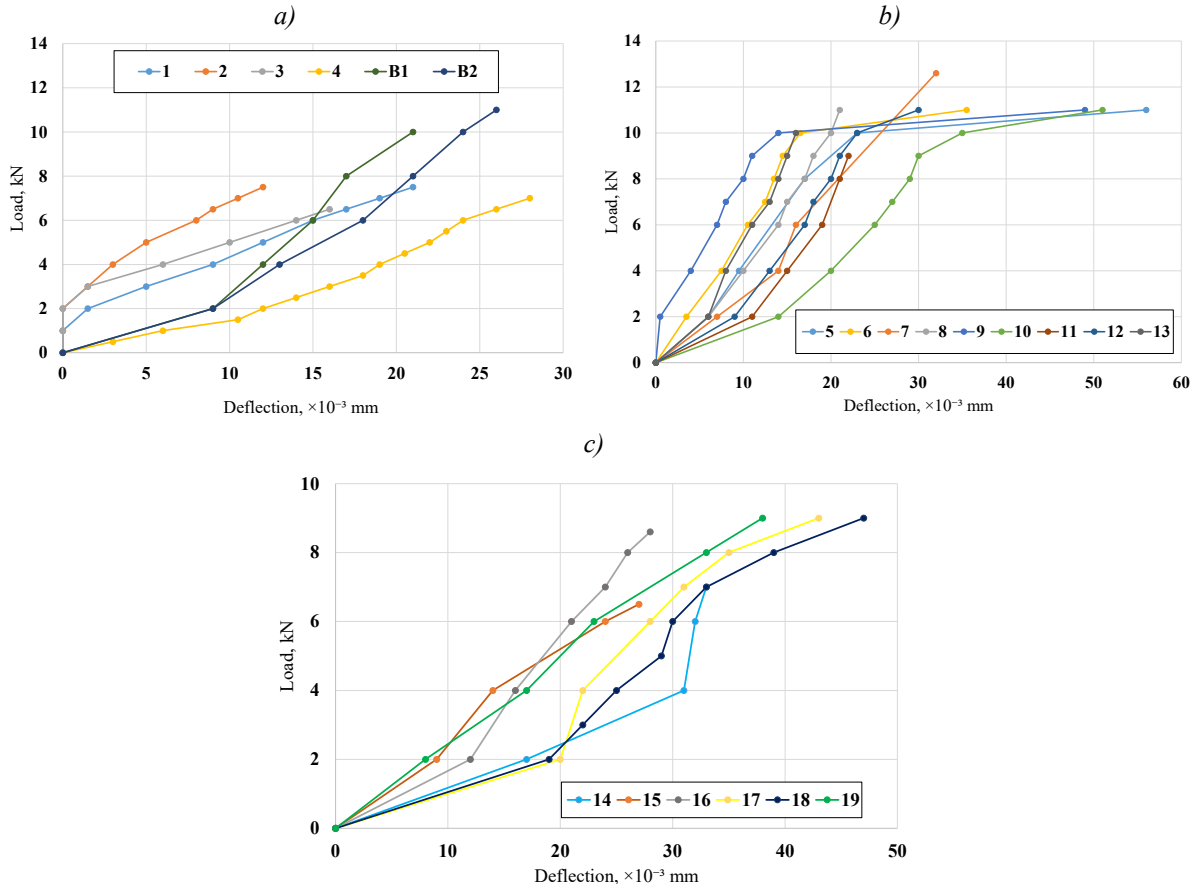


**Figure 6 - Experimental load–deflection diagrams F–w for beams: (a) series U; (b) series M; (c) series M90.**

To interpret the experimental results, three-dimensional numerical modelling of the flexural beams was carried out in the software package LIRA-FEM 2024. The model geometry reproduced the tested

beams: a rectangular cross-section of 100×100 mm and a span length of 400 mm. The solid model was built using a regular mesh of cubic finite elements with a size of 5×5×5 mm (Fig. 7).

The expanded metal sheet was modelled as a separate material connected node-to-node with the concrete volume. A piecewise-linear symmetric stress–strain law for steel was adopted: an initial elastic modulus of about 210.0 MPa, a yield strength in tension and compression of about 175 MPa at a strain of approximately 0.0008, and a subsequent increase in stress up to about 290 MPa at a strain of about 0.025. The density and Poisson's ratio were taken according to the properties of low-carbon steel 08kp.

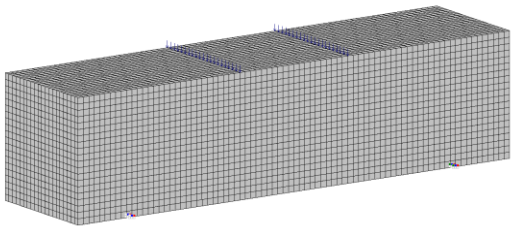

**Figure 7 – Computational geometry and finite-element mesh of the three-dimensional model of the 3D-printed beam in LIRA-FEM 2024**

The expanded metal sheet was modelled as a separate material connected node-to-node with the concrete volume. A piecewise-linear symmetric stress–strain law for steel was adopted: an initial elastic modulus of about 210.0 MPa, a yield strength in tension and compression of about 175 MPa at a strain of approximately 0.0008, and a subsequent increase in stress up to about 290 MPa at a strain of about 0.025. The density and Poisson's ratio were taken according to the properties of low-carbon steel 08kp.

The concrete material was defined as an isotropic three-dimensional material with physical nonlinearity. For the main material, a curved stress–strain relationship of the Eurocode 2 type was used, corresponding to concrete class C16/20. The analysis was performed with physical nonlinearity using an incremental–iterative procedure up to the ultimate failure stage. The first loading step corresponded to a preliminary elastic stage. Subsequently, flexural loading was applied in accordance with the test scheme: two lines of concentrated forces on the top surface located at a distance of approximately one third of the span from the supports, 7.5 kN in each line, giving a total of 15 kN. These forces were distributed along lines across the full width of the beam. For the second loading stage, 30 equal load increments were specified. The calculations were continued until loss of convergence and the appearance of large non-proportional deformations, which was interpreted as reaching the failure stage in accordance with the experimental observations.

The ultimate load obtained from the model (Fig. 8a) is about 7.5 kN, which lies well within the range of experimental failure loads of 7–9 kN for specimens 1–4. Thus, the difference between the mean experimental value and the numerical result does not exceed approximately 5–10 %. The shape of the numerical F–w diagram reproduces the main stages of the experiment: an almost linear stage up to first cracking, a noticeable reduction in stiffness after crack formation, further stiffness degradation and attainment of the maximum load. After the peak, the analysis stops due to loss of convergence (large non-proportional deformations), which corresponds to the observed failure mode in the tests.

For the reinforced specimens of series M, the FE model predicts an ultimate load of about 11.5 kN (Fig. 9), which practically coincides with the mean experimental level (~11–12.6 kN for specimens 5–13). The difference between the numerical result and the tests is also within about 10 %. Comparison of the F–w curves shows that the model correctly reproduces the increase in initial stiffness and the higher load-bearing capacity compared with series U. A characteristic feature is a flatter segment after the formation of the first crack, which corresponds to the energy-absorbing action of the thin sheet that partially restrains crack opening. It should also be noted that, in the "load–deflection" diagrams, the FE curves are significantly shifted to the right relative to the experimental ones. For loads of 7.0–11.0 kN, the numerical model gives mid-span deflections approximately 3–5 times larger than those obtained in the tests, whereas the ultimate loads practically coincide.

*a)* *b)*

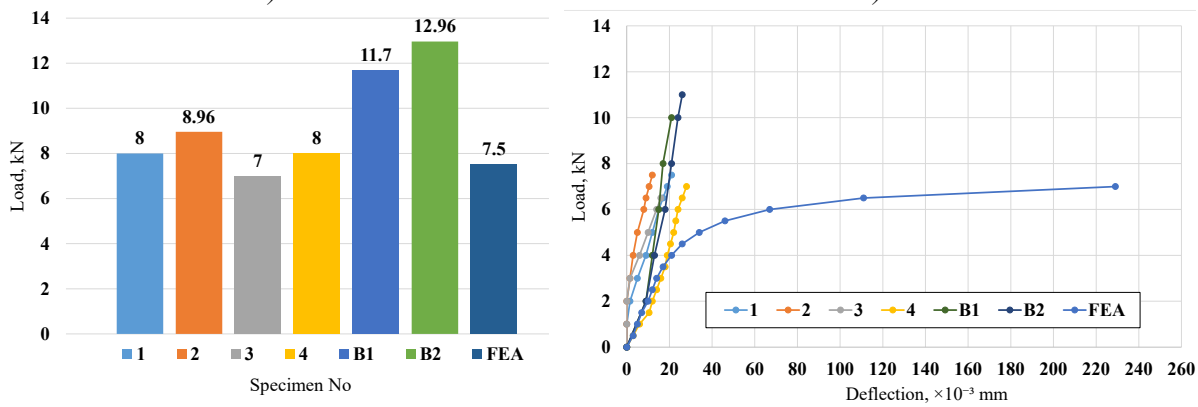


**Figure 8 – Comparison of experimental data for series U with the FE model: (a) failure loads; (b) load–deflection diagrams F–w**

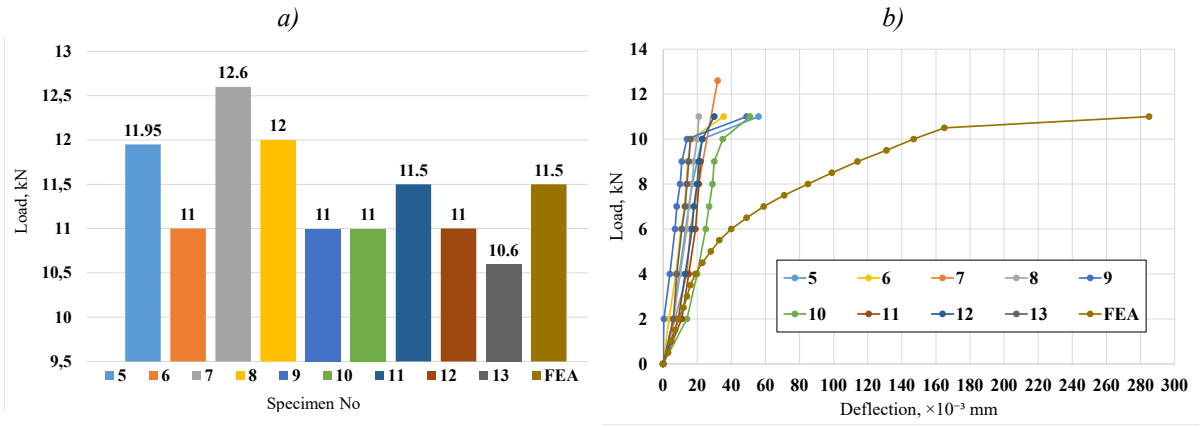


**Figure 9 – Comparison of experimental data for series M with the FE model: (a) failure loads; (b) load–deflection diagrams F–w**

This indicates that the adopted verification model slightly underestimates the beam's flexural stiffness, while reproducing its load-bearing capacity with good accuracy.

The isolines of the principal tensile stress $\sigma_1$ for the beam representing series M show stress concentrations in the bottom zone under the loading lines and in the strip occupied by the sheet.

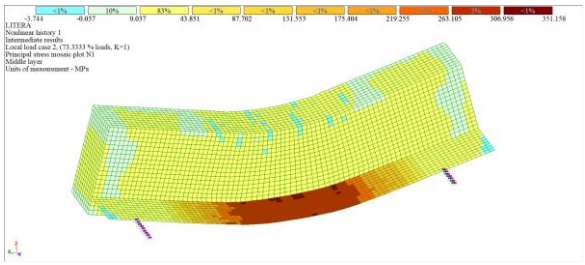

**Figure 10 – Distribution of principal tensile stresses $\sigma_1$ in the numerical model of a beam with correctly oriented expanded metal sheet (series M).**

**Conclusions.**

Based on the results of the flexural tests and numerical modelling of beams made of 3D-printed concrete reinforced with expanded metal sheet, the following conclusions can be drawn.

The geometry of experimental beams made of 3D-printed concrete was developed and a series of four-point bending tests was carried out. A three-dimensional finite-element model accounting for material physical nonlinearity was constructed and verified against the tests.

For beams of series U, the corresponding equivalent axial tensile stress is $f_{c,tk}$≈1,18 MPa, which is about ≈ 40 % lower than the mean normative value $f_{ctm}$≈1.9 MPa for concrete C16/20.

Introducing a sheet with a favourable cell orientation (series M) increases the failure load and the calculated flexural tensile strength by approximately 30–40 % compared with the unreinforced series U. At the same time, the deflection at failure and the area under the load–deflection curve increase, indicating a softer quasi-plastic response and higher fracture energy. This effect is achieved at a very low equivalent reinforcement ratio (sheet thickness $t_{eq}$≈0,17 mm in the tension zone). With a higher reinforcement ratio and ensured composite action between the steel sheet and 3DCP, even greater values of load-bearing capacity may be expected.

For beams of series M90 (sheet rotated by 90°), the mean failure loads and the shapes of the load–deflection curves remain close to those of the unreinforced beams U. Failure is governed predominantly by delamination along the mesh and debonding of the sheet from the concrete without the formation of effective crack-bridging ties. This indicates that the efficiency of this type of reinforcement is critically dependent on the orientation of the sheet relative to the direction of the principal tensile stresses.

The finite-element model correctly reproduces the ultimate load-bearing capacity but overestimates the deflections. For the unreinforced beams U, the numerical ultimate load $F_{u,mod}$≈7.5 kN falls within the range of experimental failure loads of 7–9 kN; the difference between the mean experimental value and the model does not exceed about 5–10%. For the reinforced beams of series M, the model gives $F_{u,mod}$ ≈ 11.5 kN at experimental values of ≈11–12.6 kN, i.e. the discrepancy is also within ≈10%. At the same time, for loads of 7–11 kN the computed mid-span deflections are approximately 3–5 times larger than the measured ones. This indicates that the adopted verification model slightly underestimates the beam's flexural stiffness at the service-load stage, while reproducing its load-bearing capacity with good accuracy, and therefore requires further calibration of the stress–strain relationships.

The identified reduction in equivalent axial tensile strength of 3D-printed concrete by about 40 % relative to the normative values for C16/20, together with the 30–40 % increase in beam load-bearing capacity due to the correctly oriented expanded metal sheet, provide the necessary quantitative basis for scaling the solution up to thin-walled panels and ribbed elements of permanent formwork. This data can be directly used as

design benchmarks for frame systems in which 3D-printed concrete works in tension in combination with thin steel sheet reinforcement.

## References


1. Buswell, R. A., De Silva, W. L., Jones, S. Z., & Dirrenberger, J. (2018). 3D printing using concrete extrusion: A roadmap for research. *Cement and Concrete Research, 112*, 37–49. https://doi.org/10.1016/j.cemconres.2018.05.006.
2. Wangler, T., Roussel, N., Bos, F. P., Salet, T. A. M., & Flatt, R. J. (2019). Digital concrete: A review. *Cement and Concrete Research, 123*, 105780. https://doi.org/10.1016/j.cemconres.2019.105780.
3. Mechtcherine, V., Bos, F. P., Perrot, A., Da Silva, W. R. L., Nerella, V. N., Fataei, S., Wolfs, R. J. M., Sonebi, M., & Roussel, N. (2020). Extrusion-based additive manufacturing with cement-based materials—Production steps, processes and their underlying physics: A review. *Cement and Concrete Research, 132*, 106037. https://doi.org/10.1016/j.cemconres.2020.106037
4. Rehman, A. U., & Kim, J.-H. (2021). 3D concrete printing: A systematic review of rheology, mix designs, mechanical, microstructural and durability characteristics. *Materials, 14*(14), 3800. https://doi.org/10.3390/ma14143800.
5. Hou, S., Duan, Z., Xiao, J., & Ye, J. (2021). A review of 3D printed concrete: Performance requirements, testing measurements and mix design. *Construction and Building Materials, 273*, 121745. https://doi.org/10.1016/j.conbuildmat.2020.121745.
6. Surehali, S. A. O., Tripathi, A., & Neithalath, N. (2023). Anisotropy in additively manufactured concrete specimens under compressive loading—Quantification of the effects of layer height and fiber reinforcement. *Materials, 16*(15), 5488. https://doi.org/10.3390/ma16155488.
7. Skibicki, S., Dvořák, R., Pazdera, L., Topolář, L., Kocáb, D., Alexa, M., Cendrowski, K., & Hoffmann, M. (2024). Anisotropic mechanical properties of 3D printed mortar determined by standard flexural and compression test and acoustic emission. *Construction and Building Materials, 452*, 138957. https://doi.org/10.1016/j.conbuildmat.2024.138957
8. Ma, G., Li, Z., Wang, L., Wang, F., & Sanjayan, J. (2019). Mechanical anisotropy of aligned fiber reinforced composite for extrusion-based 3D printing. *Construction and Building Materials, 202*, 770–783. https://doi.org/10.1016/j.conbuildmat.2019.01.008.
9. Liu, C., Yue, S., Zhou, C., Sun, H., Deng, S., Gao, F., & Tan, Y. (2021). Anisotropic mechanical properties of extrusion-based 3D printed layered concrete. *Journal of Materials Science, 56*, 16851–16864. https://doi.org/10.1007/s10853-021-06416-w.
10. Zhao, Y., Wu, X., Zhu, L., Yang, Z., Wang, Y., & Xi, X. (2021). The influence of polypropylene fiber on the working performance and mechanical anisotropy of 3D printing concrete. *Journal of Advanced Concrete Technology, 19*(12), 1264–1274. https://doi.org/10.3151/jact.19.1264.
11. Jiang, Q., Liu, Q., Wu, S., Zheng, H., & Sun, W. (2022). Modification effect of nanosilica and polypropylene fiber for extrusion-based 3D printing concrete: Printability and mechanical anisotropy. *Additive Manufacturing, 56*, 102944. https://doi.org/10.1016/j.addma.2022.102944

12. Feng, P., Meng, X., Chen, J.-F., & Ye, L.-P. (2015). Mechanical properties of structures 3D printed with



1. Buswell, R. A., De Silva, W. L., Jones, S. Z., & Dirrenberger, J. (2018). 3D printing using concrete extrusion: A roadmap for research. *Cement and Concrete Research, 112*, 37–49. https://doi.org/10.1016/j.cemconres.2018.05.006.
2. Wangler, T., Roussel, N., Bos, F. P., Salet, T. A. M., & Flatt, R. J. (2019). Digital concrete: A review. *Cement and Concrete Research, 123*, 105780. https://doi.org/10.1016/j.cemconres.2019.105780.
3. Mechtcherine, V., Bos, F. P., Perrot, A., Da Silva, W. R. L., Nerella, V. N., Fataei, S., Wolfs, R. J. M., Sonebi, M., & Roussel, N. (2020). Extrusion-based additive manufacturing with cement-based materials—Production steps, processes and their underlying physics: A review. *Cement and Concrete Research, 132*, 106037. https://doi.org/10.1016/j.cemconres.2020.106037
4. Rehman, A. U., & Kim, J.-H. (2021). 3D concrete printing: A systematic review of rheology, mix designs, mechanical, microstructural and durability characteristics. *Materials, 14*(14), 3800. https://doi.org/10.3390/ma14143800.
5. Hou, S., Duan, Z., Xiao, J., & Ye, J. (2021). A review of 3D printed concrete: Performance requirements, testing measurements and mix design. *Construction and Building Materials, 273*, 121745. https://doi.org/10.1016/j.conbuildmat.2020.121745.
6. Surehali, S. A. O., Tripathi, A., & Neithalath, N. (2023). Anisotropy in additively manufactured concrete specimens under compressive loading—Quantification of the effects of layer height and fiber reinforcement. *Materials, 16*(15), 5488. https://doi.org/10.3390/ma16155488.
7. Skibicki, S., Dvořák, R., Pazdera, L., Topolář, L., Kocáb, D., Alexa, M., Cendrowski, K., & Hoffmann, M. (2024). Anisotropic mechanical properties of 3D printed mortar determined by standard flexural and compression test and acoustic emission. *Construction and Building Materials, 452*, 138957. https://doi.org/10.1016/j.conbuildmat.2024.138957
8. Ma, G., Li, Z., Wang, L., Wang, F., & Sanjayan, J. (2019). Mechanical anisotropy of aligned fiber reinforced composite for extrusion-based 3D printing. *Construction and Building Materials, 202*, 770–783. https://doi.org/10.1016/j.conbuildmat.2019.01.008.
9. Liu, C., Yue, S., Zhou, C., Sun, H., Deng, S., Gao, F., & Tan, Y. (2021). Anisotropic mechanical properties of extrusion-based 3D printed layered concrete. *Journal of Materials Science, 56*, 16851–16864. https://doi.org/10.1007/s10853-021-06416-w.
10. Zhao, Y., Wu, X., Zhu, L., Yang, Z., Wang, Y., & Xi, X. (2021). The influence of polypropylene fiber on the working performance and mechanical anisotropy of 3D printing concrete. *Journal of Advanced Concrete Technology, 19*(12), 1264–1274. https://doi.org/10.3151/jact.19.1264.
11. Jiang, Q., Liu, Q., Wu, S., Zheng, H., & Sun, W. (2022). Modification effect of nanosilica and polypropylene fiber for extrusion-based 3D printing concrete: Printability and mechanical anisotropy. *Additive Manufacturing, 56*, 102944. https://doi.org/10.1016/j.addma.2022.102944
12. Feng, P., Meng, X., Chen, J.-F., & Ye, L.-P. (2015). Mechanical properties of structures 3D printed with

cementitious powders. *Construction and Building Materials, 93*, 486–497. https://doi.org/10.1016/j.conbuildmat.2015.05.132

13. Le, T. T., Austin, S. A., Lim, S., Buswell, R. A., Law, R., Gibb, A. G. F., & Thorpe, T. (2012). Hardened properties of high-performance printing concrete. *Cement and Concrete Research, 42*(3), 558–566. https://doi.org/10.1016/j.cemconres.2011.12.003

14. Wolfs, R. J. M., Bos, F. P., & Salet, T. A. M. (2018). Early age mechanical behaviour of 3D printed concrete: Numerical modelling and experimental testing. *Cement and Concrete Research, 106*, 103–116. https://doi.org/10.1016/j.cemconres.2018.02.001

15. Nerella, V. N., Hempel, S., & Mechtcherine, V. (2019). Effects of layer-interface properties on mechanical performance of concrete elements produced by extrusion-based 3D-printing. *Construction and Building Materials, 205*, 586–601. https://doi.org/10.1016/j.conbuildmat.2019.01.235

16. Sanjayan, J. G., Nematollahi, B., Xia, M., & Marchment, T. (2018). Effect of surface moisture on inter-layer strength of 3D printed concrete. *Construction and Building Materials, 172*, 468–475. https://doi.org/10.1016/j.conbuildmat.2018.03.232

17. Hosseini, E., Zakertabrizi, M., Korayem, A. B., & Xu, G. (2019). A novel method to enhance the interlayer bonding of 3D printing concrete: An experimental and computational investigation. *Cement and Concrete Composites, 99*, 112–119. https://doi.org/10.1016/j.cemconcomp.2019.03.008

18. van den Heever, M., du Plessis, A., & van Zijl, G. (2022). Evaluating the effects of porosity on the mechanical properties of extrusion-based 3D printed concrete. *Cement and Concrete Research, 153*, 106695. https://doi.org/10.1016/j.cemconres.2021.106695

19. Ma, L., Zhang, Q., Lombois-Burger, H., Jia, Z., Zhang, Z., Niu, G., & Zhang, Y. (2022). Pore structure, internal relative humidity, and fiber orientation of 3D printed concrete with polypropylene fiber and their relation with shrinkage. *Journal of Building Engineering, 61*, 105250. https://doi.org/10.1016/j.jobe.2022.105250

20. Ding, T., Xiao, J., Zou, S., & Zhou, X. (2020). Anisotropic behavior in bending of 3D printed concrete reinforced with fibers. *Composite Structures, 254*, 112808. https://doi.org/10.1016/j.compstruct.2020.112808

21. Xiao, J., Liu, H., & Ding, T. (2021). Finite element analysis on the anisotropic behavior of 3D printed concrete under compression and flexure. *Additive Manufacturing, 39*, 101712. https://doi.org/10.1016/j.addma.2020.101712

22. Jipa, A., & Dillenburger, B. (2022). 3D printed formwork for concrete: State-of-the-art, opportunities, challenges, and applications. *3D Printing and Additive Manufacturing, 9*(2), 84–107. https://doi.org/10.1089/3dp.2021.0024

23. Mata-Falcón, J., Bischof, P., Huber, T., Anton, A., Burger, J., Ranaudo, F., Jipa, A., Gebhard, L., Reiter, L., Lloret-Fritschi, E., Van Mele, T., Block, P., Gramazio, F., Kohler, M., Dillenburger, B., Wangler, T., & Kaufmann, W. (2022). Digitally fabricated ribbed concrete floor slabs: A sustainable solution for construction. *RILEM Technical Letters, 7*, 68–78. https://doi.org/10.21809/rilemtechlett.2022.161

24. Burger, J., Huber, T., Lloret-Fritschi, E., Mata-Falcón, J., et al. (2022). Design and fabrication of optimised ribbed concrete floor slabs using large scale 3D printed formwork. *Automation in Construction, 144*, 104599. https://doi.org/10.1016/j.autcon.2022.104599

25. ДСТУ Б В.2.7-214:2009. Будівельні матеріали. Бетони. Методи визначення міцності за контрольними

cementitious powders. *Construction and Building Materials, 93*, 486–497. https://doi.org/10.1016/j.conbuildmat.2015.05.132

13. Le, T. T., Austin, S. A., Lim, S., Buswell, R. A., Law, R., Gibb, A. G. F., & Thorpe, T. (2012). Hardened properties of high-performance printing concrete. *Cement and Concrete Research, 42*(3), 558–566. https://doi.org/10.1016/j.cemconres.2011.12.003

14. Wolfs, R. J. M., Bos, F. P., & Salet, T. A. M. (2018). Early age mechanical behaviour of 3D printed concrete: Numerical modelling and experimental testing. *Cement and Concrete Research, 106*, 103–116. https://doi.org/10.1016/j.cemconres.2018.02.001

15. Nerella, V. N., Hempel, S., & Mechtcherine, V. (2019). Effects of layer-interface properties on mechanical performance of concrete elements produced by extrusion-based 3D-printing. *Construction and Building Materials, 205*, 586–601. https://doi.org/10.1016/j.conbuildmat.2019.01.235

16. Sanjayan, J. G., Nematollahi, B., Xia, M., & Marchment, T. (2018). Effect of surface moisture on inter-layer strength of 3D printed concrete. *Construction and Building Materials, 172*, 468–475. https://doi.org/10.1016/j.conbuildmat.2018.03.232

17. Hosseini, E., Zakertabrizi, M., Korayem, A. B., & Xu, G. (2019). A novel method to enhance the interlayer bonding of 3D printing concrete: An experimental and computational investigation. *Cement and Concrete Composites, 99*, 112–119. https://doi.org/10.1016/j.cemconcomp.2019.03.008

18. van den Heever, M., du Plessis, A., & van Zijl, G. (2022). Evaluating the effects of porosity on the mechanical properties of extrusion-based 3D printed concrete. *Cement and Concrete Research, 153*, 106695. https://doi.org/10.1016/j.cemconres.2021.106695

19. Ma, L., Zhang, Q., Lombois-Burger, H., Jia, Z., Zhang, Z., Niu, G., & Zhang, Y. (2022). Pore structure, internal relative humidity, and fiber orientation of 3D printed concrete with polypropylene fiber and their relation with shrinkage. *Journal of Building Engineering, 61*, 105250. https://doi.org/10.1016/j.jobe.2022.105250

20. Ding, T., Xiao, J., Zou, S., & Zhou, X. (2020). Anisotropic behavior in bending of 3D printed concrete reinforced with fibers. *Composite Structures, 254*, 112808. https://doi.org/10.1016/j.compstruct.2020.112808

21. Xiao, J., Liu, H., & Ding, T. (2021). Finite element analysis on the anisotropic behavior of 3D printed concrete under compression and flexure. *Additive Manufacturing, 39*, 101712. https://doi.org/10.1016/j.addma.2020.101712

22. Jipa, A., & Dillenburger, B. (2022). 3D printed formwork for concrete: State-of-the-art, opportunities, challenges, and applications. *3D Printing and Additive Manufacturing, 9*(2), 84–107. https://doi.org/10.1089/3dp.2021.0024

23. Mata-Falcón, J., Bischof, P., Huber, T., Anton, A., Burger, J., Ranaudo, F., Jipa, A., Gebhard, L., Reiter, L., Lloret-Fritschi, E., Van Mele, T., Block, P., Gramazio, F., Kohler, M., Dillenburger, B., Wangler, T., & Kaufmann, W. (2022). Digitally fabricated ribbed concrete floor slabs: A sustainable solution for construction. *RILEM Technical Letters, 7*, 68–78. https://doi.org/10.21809/rilemtechlett.2022.161

24. Burger, J., Huber, T., Lloret-Fritschi, E., Mata-Falcón, J., et al. (2022). Design and fabrication of optimised ribbed concrete floor slabs using large scale 3D printed formwork. *Automation in Construction, 144*, 104599. https://doi.org/10.1016/j.autcon.2022.104599

25. UkrNDNC. (2009). *DSTU B V.2.7-214:2009. Concretes. Methods of determination of strength by control*

зразками. Київ: Мінрегіонбуд України, 2010. 43 с.

26. LIRALAND Group. LIRA-FEM – finite element structural analysis software: official website. URL: https://www.liraland.com/.

27. Резнік П. О., Петренко Д. Г., Володимиров А. В., Алатаєв Д. А., Максименко В. О. Анізотропія міцності 3D-друкованого бетону: експериментальне дослідження та статистичний аналіз. Науковий вісник будівництва. 2025. Вип. 112, № 1. С. 248–255. https://doi.org/10.33042/2311-7257.2025.112.1.30

28. ДБН В.2.6-98:2009. Конструкції будинків і споруд. Бетонні та залізобетонні конструкції. Основні положення. Зі Зміною № 1. Київ: Мінрегіонбуд України, 2011.

29. Gebhard, L., van der Woerd, J., Bos, F., & Salet, T. (2021). Structural behaviour of 3D printed concrete beams with various reinforcement strategies. *Engineering Structures, 240*, 112380. https://doi.org/10.1016/j.engstruct.2021.112380

30. Liu, X., Dobrzanski, J., Kolawole, J. T., & Buswell, R. (2025). Factors affecting the flexural performance of reinforced 3D printed concrete beams. *Engineering Structures, 337*, 120497. https://doi.org/10.1016/j.engstruct.2025.120497

*samples* [State standard of Ukraine]. Ukrainian Research and Training Center for Standardization, Certification and Quality.

26. LIRALAND Group. (n.d.). *LIRA-FEM: Structural analysis software* [Computer software]. Retrieved from https://www.liraland.com/lira/

27. Reznik, P. A., Petrenko, D. H., Volodymyrov, A. V., Alataiev, D. A., & Maksymenko, V. O. (2025). Strength anisotropy of 3D-printed concrete: Experimental investigation and statistical analysis. *Scientific Bulletin of Construction, 112*(1), 248–255. https://doi.org/10.33042/2311-7257.2025.112.1.30

28. Ministry of Regional Development and Construction of Ukraine. (2009). *DBN V.2.6-98:2009. Concrete and reinforced concrete structures. Basic provisions* (with Amendment No. 1, effective from 2020) [State building code of Ukraine]. Minregionbud of Ukraine.

29. Gebhard, L., van der Woerd, J., Bos, F., & Salet, T. (2021). Structural behaviour of 3D printed concrete beams with various reinforcement strategies. *Engineering Structures, 240*, 112380. https://doi.org/10.1016/j.engstruct.2021.112380

30. Liu, X., Dobrzanski, J., Kolawole, J. T., & Buswell, R. (2025). Factors affecting the flexural performance of reinforced 3D printed concrete beams. *Engineering Structures, 337*, 120497. https://doi.org/10.1016/j.engstruct.2025.120497

| Suggested Citation: | |
|---|---|
| APA style | Reznik , P., Petrenko, D., Volodymyrov, A., & Alataiev, D. (2025). Flexural Behaviour of 3DCP Beams with Expanded Metal Sheet Reinforcement: Experimental Investigation and Numerical Verification. *Academic Journal Industrial Machine Building Civil Engineering*, *1* (64), 119–129. https://doi.org/10.26906/znp.2025.64.4144 |
| DSTU style | Flexural Behaviour of 3DCP Beams with Expanded Metal Sheet Reinforcement: Experimental Investigation and Numerical Verification/ P. Reznik et al. *Academic journal. Industrial Machine Building, Civil Engineering*. 2025. Vol. 64, iss. 1. P. 119–129. URL: https://doi.org/10.26906/znp.2025.64.4144. |

**Петро Резнік ***
Харківський національний університет міського господарства імені О.М. Бекетова
https://orcid.org/0000-0003-3937-6833

**Дмитро Петренко**
Харківський національний університет міського господарства імені О.М. Бекетова
https://orcid.org/0000-0002-8168-7224

**Антон Володимиров**
Харківський національний університет міського господарства імені О.М. Бекетова
https://orcid.org/0009-0001-8416-535X

**Джамалдій Алатаєв**
Харківський національний університет міського господарства імені О.М. Бекетова
https://orcid.org/0000-0003-1570-8469

# Згинальна робота 3D-друкованих бетонних балок з армуванням просічно-витяжним листом: експериментальне дослідження та чисельна верифікація

Аннотація. У статті наведено результати експериментальних та числових досліджень згинальної роботи балок із бетону 3D-друку (3DCP), армованих просічно-витяжним сталевим листом (ПВЛ). Призматичні зразки розміром 100×100×400 мм із 3DCP та контрольного бетону С20/25 випробовували на згин за схемою чотириточкового навантаження відповідно до ДСТУ Б В.2.7-214:2009 із реєстрацією діаграм «навантаження–прогин» і деформацій у стиснутій та розтягнутій зонах. Встановлено, що використана 3D-друкована суміш, яка за міцністю на стиск відповідає класу С16/20, має приведену осьову міцність на розтяг лише 1.02–1.25 МПа, тобто приблизно на 30–45 % меншу за нормативне значення fctm для бетону С16/20, що зумовлює знижену тріщиностійкість. За правильної орієнтації довгої діагоналі ПВЛ уздовж напрямку екструзії руйнівне навантаження та згинальна тріщиностійкість балок зростають на 30–40 %, а характер роботи переходить до більш пластичного, енергоємного. Для серії з листом, повернутим на 90°, додатковий ефект практично відсутній через розшарування вздовж ПВЛ. Побудована в LIRA-FEM 2024 тривимірна скінченно-елементна модель з фізично нелінійним бетоном відтворює граничну несучу здатність балок з похибкою близько 5–10 %, хоча занижує згинальну жорсткість, що потребує подальшого уточнення моделей деформування та розширення досліджень для тонкостінних елементів незнімної опалубки.

Ключові слова: бетони 3D-друку (3DCP); міцність на розтяг при згині; просічно-витяжний лист; скінченно-елементне моделювання; незнімна опалубка..

*Адреса для листування E-mail: Petro.Reznik@kname.edu.ua

| Надіслано до редакції: | 16.05.2025 | Прийнято до друку після рецензування: | 06.06.2025 | Опубліковано (оприлюднено): | 26.06.2025 |
|---|---|---|---|---|---|